

Quantum Simulating Lattice Gauge Theories with Optical Lattices

Yannick Meurice

University of Iowa

Work done with Philipp Preiss (Heidelberg), Shan-Wen Tsai (UCR), Judah Unmuth-Yockey (U. Iowa/Syracuse), Li-Ping Yang (Chongqing U.) and Jin Zhang (UCR)

Near-term Applications of Quantum Computing

Fermilab, November 7, 2017



Talk Content

- Main Message
- Overview, motivations from the lattice gauge theory point of view
- Quantum simulations on optical lattices
- The Tensor Renormalization Group (TRG) method (summary)
- The $O(2)$ model
- Entanglement entropy and central charge
- The Abelian Higgs model in 1+1 dimensions
- Polyakov's loop
- Corresponding Bose Hubbard models
- Optical lattice implementations
- Ladders of Rydberg atoms
- A proof of principle: data collapse for the quantum Ising model
- Conclusions



Main Message

- We have reformulated the **lattice Abelian Higgs model** (scalar QED) in 1 space + 1 time dimension using the **Tensor Renormalization Group** method.
- The reformulation is **gauge invariant** and connects smoothly the classical Lagrangian formulation used by lattice gauge theorists and the quantum Hamiltonian method used in condensed matter and for **quantum simulations**.
- In the $O(2)$ limit we can add a chemical potential and reach a superfluid phase at small hopping. The entanglement entropy scales like in Conformal Field Theory ($(c/8) \ln(N)$) which could be checked **using current experiments quantum simulating the Bose-Hubbard (BH) model**.
- We propose to use **BH Hamiltonians with a ladder structure** as quantum simulators.
- Recent experimental progress allows this setup and we propose data collapse checks for small systems (FSS).



Important Lattice QCD problems/questions

- A common problem to practical lattice QCD calculations: large box size/small lattice spacing = many lattice sites.
- The problem gets more acute for many flavors with small masses (composite Higgs models?). Existence of non-trivial IR fixed points for enough flavors (e.g. $SU(3)$ with 12 massless quarks)? What are the remnants of the expected CFT on the lattice? Is there a topological picture? Again, lattices used in numerical calculations always seem too small.
- Finite density calculations: sign problem (MC calculations with complex actions are only possible if the complex part is small enough to be handled with reweighing).
- Real time evolution: requires detailed information about the Hamiltonian and the states which is usually not available from conventional MC simulations at Euclidean time.



Quantum simulations?

We need to start with something simple!



Figure: Mike Creutz's calculator used for a Z_2 gauge theory on a 3^4 lattice (circa 1979).

30+ years later



The Fermilab cluster, accurate estimates of $|V_{ub}|$, $g - 2$, nuclear form factors for neutrino experiments, exploration of the boundary of the conformal window

...

PHYSICAL REVIEW D **92**, 014024 (2015)

$|V_{ub}|$ from $B \rightarrow \pi \ell \nu$ decays and $(2+1)$ -flavor lattice QCD

Jon. A. Bailey,¹ A. Bazavov,^{2*} C. Bernard,³ C. M. Bouchard,^{4,5} C. DeTar,⁶ D. Du,^{7,8,†} A. X. El-Khadra,⁷ J. Foley,⁶ E. D. Freeland,¹⁰ E. Gámiz,¹⁰ Steven Gottlieb,¹¹ U. M. Heller,¹² J. Komijani,¹ A. S. Kronfeld,^{13,14} J. Lailho,¹ L. Levkova,¹⁵ Yuzhi Liu,¹⁵ P. B. Mackenzie,¹⁵ Y. Meurice,¹⁶ E. Neil,^{15,17} Si-Wei Qiu,¹² N. Simone,¹³ R. Sugar,¹⁸ D. Toussaint,¹⁹ R. S. Van de Water,¹³ and R. Zhou¹³

(Fermilab Lattice and MILC collaborations)

¹Department of Physics and Astronomy, Seoul National University, Seoul, South Korea

²Physics Department, Brookhaven National Laboratory, Upton, New York, USA

³Department of Physics, Washington University, St. Louis, Missouri, USA

⁴Department of Physics, The Ohio State University, Columbus, Ohio, USA

⁵Physics Department, College of William and Mary, Williamsburg, Virginia, USA

⁶Department of Physics and Astronomy, University of Utah, Salt Lake City, Utah, USA

⁷Department of Physics, University of Illinois, Urbana, Illinois, USA

⁸Department of Physics, Syracuse University, Syracuse, New York, USA

⁹Liberal Arts Department, School of the Art Institute of Chicago, Chicago, Illinois, USA

¹⁰CAFPE and Departamento de Física Teórica y del Cosmos, Universidad de Granada, Granada, Spain

¹¹Department of Physics, Indiana University, Bloomington, Indiana, USA

¹²American Physical Society, Ridge, New York, USA

¹³Fermi National Accelerator Laboratory, Batavia, Illinois, USA

¹⁴Institute for Advanced Study, Technische Universität München, Garching, Germany

¹⁵Department of Physics, University of Colorado, Boulder, Colorado, USA

¹⁶Department of Physics and Astronomy, University of Iowa, Iowa City, Iowa, USA

¹⁷RKEN-BNL Research Center, Brookhaven National Laboratory, Upton, New York, USA

¹⁸Department of Physics, University of California, Santa Barbara, California, USA

¹⁹Physics Department, University of Arizona, Tucson, Arizona, USA

(Received 3 April 2015; published 23 July 2015)

We present a lattice-QCD calculation of the $B \rightarrow \pi \ell \nu$ semileptonic form factors and a new determination of the CKM matrix element $|V_{ub}|$. We use the MILC asqtad $(2+1)$ -flavor lattice configurations at four lattice spacings and light-quark masses down to 1/20 of the physical strange-quark mass. We extrapolate the lattice form factors to the continuum using staggered chiral perturbation theory in the hard-pion and SU(2) limits. We employ a model-independent ζ parametrization to extrapolate our lattice form factors from large-recoil momentum to the full kinematic range. We introduce a new functional method to propagate information from the chiral-continuum extrapolation to the ζ expansion. We present our results together with a complete systematic error budget, including a covariance matrix to enable the combination of our form factors with other lattice-QCD and experimental results. To obtain $|V_{ub}|$, we simultaneously fit the experimental data for the $B \rightarrow \pi \ell \nu$ differential decay rate obtained by the BABAR and Belle collaborations together with our lattice form-factor results. We find $|V_{ub}| = (3.72 \pm 0.16) \times 10^{-3}$, where the error is from the combined fit to lattice plus experiments and includes all sources of uncertainty. Our form-factor results being the QCD error on $|V_{ub}|$ to the same level as the experimental error. We also provide results for the $B \rightarrow \pi \ell \nu$ vector and scalar form factors obtained from the combined lattice and experiment fit, which are more precisely determined than from our lattice-QCD calculation alone. These results can be used in other phenomenological applications and to test other approaches to QCD.



Field theory and machine learning (Daping Du)

Daping Du

2 Following 10 Followers

Follow



Stories in
Insight Data

Other stories by Daping Du >



Daping Du in Insight Data

Nov 21, 2016 · 9 min read



Anonymization, Word Vectors and $O(n)$ model

Quantifying private information using word vector models



A first quantum calculator for the abelian Higgs model?



Figure: Left: Johannes Zeiher, a recent graduate from Immanuel Bloch's group can design ladder shaped optical lattices with nearest neighbor interactions. Right: an optical lattice experiment, once used to observe a "Higgs mode" by Bloch's group.

Quantum Simulators

- No sign problems
- Real time evolution
- Large optical lattices ($L \simeq 1000$) are part of the future
- We can do interesting experiments with small lattices
- Many interesting proposals based on the Kogut-Susskind Hamiltonian and quantum rotors (Reznik, Zohar, Cirac, Wiese, Lewenstein, Kuno, Dalmonte, Zoller, Muschick et al. and others; see Uwe's talk)
- Our approach is based on the tensor formulation of lattice gauge theory and is **manifestly gauge invariant**
- So far, the remarkable theory-experiment reached for the Bose-Hubbard model is just a source of inspiration in the context of lattice gauge theory and a proof of principle is needed



Optical lattices "computers"

Alkali-metals (Li, Na, K, Rb, Cs) have a loosely bound electron in the the outer shell. Typical choices are ^{87}Rb (a boson: 37 e^- , 37 p and 50 n) or ^6Li (a fermion: 3 e^- , 3 p and 3 n).

The polarizable cold atoms are trapped in standing waves created by counterpropagating laser beams in 1, 2 or 3 dimensions. The periodic potential is due to the dipole moment induced by the linearly polarized laser beam:

$$V(\mathbf{r}) = -(1/2)\alpha(\omega)|\mathbf{E}(\mathbf{r})|^2, \quad (1)$$

with

$$\alpha(\omega) \sim |\langle \mathbf{e} | \mathbf{d} | \mathbf{g} \rangle|^2 / \hbar(\omega_0 - \omega_L). \quad (2)$$



Example, orders of magnitude

3D lattice potential with a cubic symmetry using 3 mutually orthogonal laser beams of the same wavelength λ_L . The periodic potential is

$$V(x, y, z) = V_0(\sin^2(kx) + \sin^2(ky) + \sin^2(kz)) ,$$

with $k = 2\pi/\lambda_L$. The lattice spacing is $a = \lambda_L/2$.

The depth of the potential V_0 is measured in units of the recoil energy $E_r \equiv (\hbar k)^2/2m_{\text{atom}}$ and can be tuned continuously by changing the intensity of the laser.

For Rubidium atoms with $\lambda_L = 856\text{nm}$, the recoil energy is $1.3 \times 10^{-11} \text{ eV} \simeq k_B 1.5 \times 10^{-7} \text{ K}$. The critical temperature for Bose condensation in Rubidium with a specific volume of $(\lambda_L/2)^3$ is close to 10^{-7} K according to the ideal gas formula. The recoil momentum is $1.5\text{eV}/c$ and the recoil velocity about 5 mm/s .

Of the order of $N_{\text{atoms}} \simeq 65^3$ can be used. Assuming one atom per site, the physical size of the lattice is of the order of $30 \mu\text{m}$.

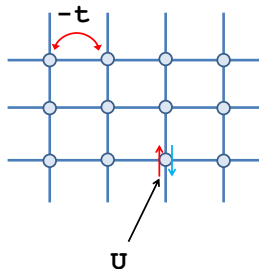


The Bose-Hubbard model

The Hubbard model Hamiltonian is

$$H = -t \sum_{\langle i,j \rangle} (a_i^\dagger a_j + h.c.) + \frac{U}{2} \sum_i n_i^2 - \mu \sum_i n_i$$

where t characterizes the tunneling between nearest neighbor sites and U controls the onsite Coulomb repulsion. These interactions can be approximately recreated with the atoms trapped in an optical lattice.



Phase diagram of the Bose Hubbard model

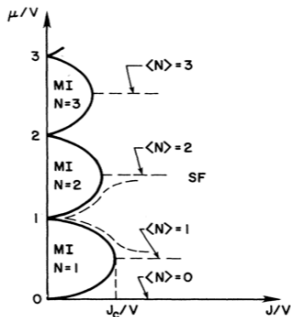


FIG. 1. Zero-temperature phase diagram for the lattice model of interacting bosons, (2.1), in the absence of disorder. For an integer number of bosons per site the superfluid phase (SF) is unstable to a Mott insulating (MI) phase at small J/V .

Figure: M. P. A. Fisher et al. Phys. Rev. B 40, 546 (1989) .

Insulator-Superfluid transition

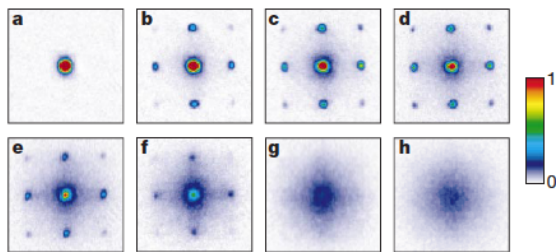


Figure 2 Absorption images of multiple matter wave interference patterns. These were obtained after suddenly releasing the atoms from an optical lattice potential with different potential depths V_0 after a time of flight of 15 ms. Values of V_0 were: **a**, $0 E_r$; **b**, $3 E_r$; **c**, $7 E_r$; **d**, $10 E_r$; **e**, $13 E_r$; **f**, $14 E_r$; **g**, $16 E_r$; and **h**, $20 E_r$.

Figure: Observation of the superfluid to Mott insulator transition when the potential depth increases in ballistic pictures (M. Greiner et al. Nature 415, 51 (2002)).

The (high) standards: Quantum Monte Carlo vs. Experiment for BH

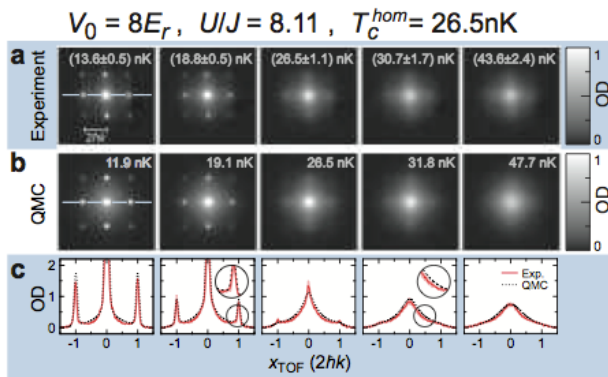
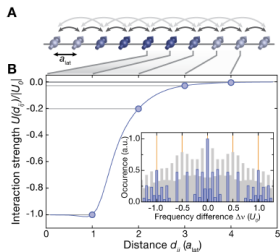


Figure: From S. Trotzky, L. Pollet, F. Gerbier, U. Schnorrberger, I. Bloch, N.V. Prokof'ev, B. Svistunov, M. Troyer Nature Phys. 6, 998-1004 (2010)

Recent experimental progress



High-resolution detection

Quantum gas microscopes enable the high-resolution fluorescence detection of atoms in single sites of a two-dimensional layer of optical lattices. The lattice spacing is small (typically $0.5\ \mu\text{m}$), such that the atoms can move through the lattice by tunneling with amplitude t . Additionally, they interact with each other with strength U when multiple atoms meet at the same lattice site. Quantum gas microscopy can provide access to single snapshots of the locally resolved atomic density in strongly correlated many-body systems.

A typical fluorescence image is shown at the lower left, where the fluorescence strength is encoded in the color scale from black over red to yellow. Thanks to the underlying lattice (white dots), the single site occupation can be faithfully reconstructed even in dense areas, whereas sparse individual atoms are directly visible.

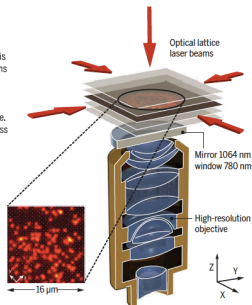


Fig. 1 Quantum gas microscopes. [Adapted from (20)]

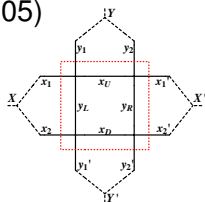
Tunable nearest neighbor interactions, Johannes Zeiher et al. arxiv 1705.08372

Quantum gas microscopes, Gross and Bloch, Science 357, 995-1001 (2017)

The Tensor Renormalization Group (TRG) method

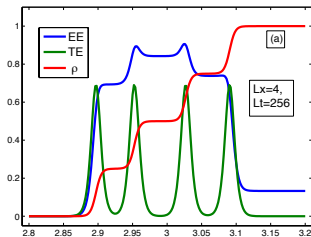
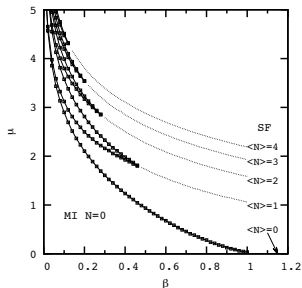
- Based on character expansions over links, plaquettes, ... $Z = \text{Tr} \prod T$ are sums over paths, surfaces ...
- **Exact** blocking (spin and gauge, PRD 88 056005)

Unique feature: the blocking separates the degrees of freedom inside the block (integrated over), from those kept to communicate with the neighboring blocks. The only approximation is the truncation in the number of "states" kept.



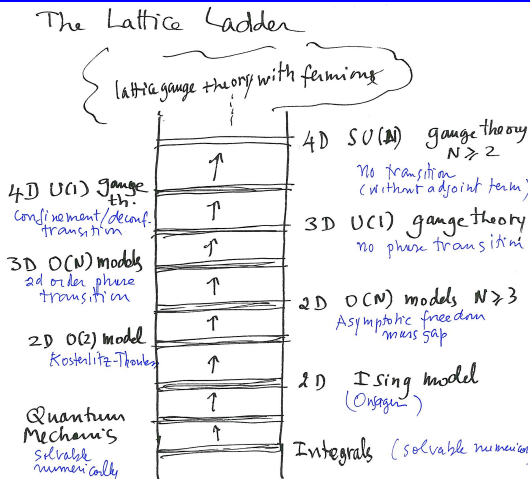
- Applies to many lattice models: Ising model, $O(2)$ model, $O(3)$ model, $SU(2)$ principal chiral model (in any dimensions), Abelian and $SU(2)$ gauge theories (1+1 and 2+1 dimensions)
- **Solution of sign problems:** complex temperature (PRD 89, 016008), chemical potential (PRA 90, 063603)
- Critical exponents of Ising (PRB 87, 064422; Kadanoff RMP 86)
- Connects easily to the **Hamiltonian picture** and provides **spectra**
- Used to design quantum simulators: $O(2)$ model (PRA 90, 063603), Abelian Higgs model (PRD 92 076003) on optical lattices

- 1+1 dimensions: phase diagram of $O(2)$ + chemical potential (PRA 90, 063603) and Entanglement entropy (PRE 93, 012138)



- Gauge invariant transfer matrix for the Abelian Higgs model in 1+1 dimensions (PRD 92 076003). This is an exact effective theory.
- Central charge of $O(2)$ in the superfluid/KT phase ($c=1$) from entanglement entropy; PRA 96 023603, PRD 96 034514 (2017).
- Polyakov loop in the Abelian Higgs model.
- Ising fermions (Grassmann version of Kaufman, in progress).
- Schwinger model: Y. Shimizu and Y. Kuramashi (\sim MPS work?) 

Climbing the lattice ladder: a "dialogue" between the TRG and sampling methods



Climbing down the lattice “ladder” (then climbing up)

- **QCD: SU(3) gauge fields + quarks**, non-perturbative, requires a 4D (3 space + 1 Euclidean time) lattice.
- **QED: U(1) photons + electrons (and positrons)**, the theory of (almost) everything, perturbative, Feynman diagrams work well for most problems.
- 3D models (spin, gauge, ...)
- **QED in 1+1 dimensions: the Schwinger model**, non-perturbative, confinement, mass gap, solvable at zero electron mass.
- **Scalar QED in 1+1 dimensions**: the Schwinger model with spinless (scalar) electrons, confinement, deconfinement at finite volume (probed with the Polyakov’s loop)?
- **O(2) model in 1+1 dimensions**: the zero gauge coupling limit of scalar QED, Kosterlitz-Thouless transition, Conformal Field Theory with $c=1$.



The $O(2)$ model with a real chemical potential μ

$$Z = \int \prod_{(x,t)} \frac{d\theta_{(x,t)}}{2\pi} e^{-S}.$$

$$\begin{aligned} S = & - \beta_\tau \sum_{(x,t)} \cos(\theta_{(x,t+1)} - \theta_{(x,t)} - i\mu) \\ & - \beta_s \sum_{(x,t)} \cos(\theta_{(x+1,t)} - \theta_{(x,t)}). \end{aligned}$$

$$\begin{aligned} Z = & \sum_{\{n\}} \prod_{(x,t)} I_{n_{(x,t),\hat{x}}}(\beta_s) I_{n_{(x,t),\hat{t}}}(\beta_\tau) e^{\mu n_{(x,t),\hat{t}}} \\ & \times \delta_{n_{(x-1,t),\hat{x}} + n_{(x,t-1),\hat{t}}, n_{(x,t),\hat{x}} + n_{(x,t),\hat{t}}}. \end{aligned}$$

For real μ the action is complex, $\beta = 1/g^2$



Worm configurations

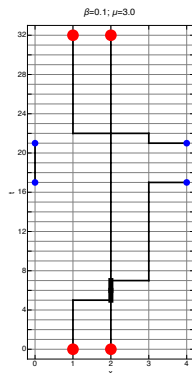


Figure: Allowed configuration of $\{n\}$ for a 4 by 32 lattice. The uncovered links on the grid have $n=0$, the more pronounced dark lines have $|n|=1$ and the wider lines have $n=2$. The dots need to be identified periodically. The time slice 5, represents a transition between $|1100\rangle$ and $|0200\rangle$. Statistical sampling of these configurations (worm algorithm, Banerjee and Chandrasekharan PRD 81) has been used to check the TRG calculations.



TRG approach of the transfer matrix

The partition function can be expressed in terms of a transfer matrix:

$$Z = \text{Tr} \mathbb{T}^{L_t} .$$

The matrix elements of \mathbb{T} can be expressed as a product of tensors associated with the sites of a time slice (fixed t) and traced over the space indices (PhysRevA.90.063603)

$$\mathbb{T}_{(n_1, n_2, \dots, n_{L_x})(n'_1, n'_2, \dots, n'_{L_x})} = \sum_{\tilde{n}_1 \tilde{n}_2 \dots \tilde{n}_{L_x}} T_{\tilde{n}_{L_x} \tilde{n}_1 n_1 n'_1}^{(1,t)} T_{\tilde{n}_1 \tilde{n}_2 n_2 n'_2}^{(2,t)} \dots T_{\tilde{n}_{L_x-1} \tilde{n}_{L_x} n_{L_x} n'_{L_x}}^{(L_x,t)}$$

with

$$T_{\tilde{n}_{x-1} \tilde{n}_x n_x n'_x}^{(x,t)} = \sqrt{I_{n_x}(\beta_\tau) I_{n'_x}(\beta_\tau) I_{\tilde{n}_{x-1}}(\beta_s) I_{\tilde{n}_x}(\beta_s) e^{\mu(n_x + n'_x)}} \delta_{\tilde{n}_{x-1} + n_x, \tilde{n}_x + n'_x}$$

The Kronecker delta function reflects the existence of a conserved current, a good quantum number ("particle number").



Coarse-graining of the transfer matrix

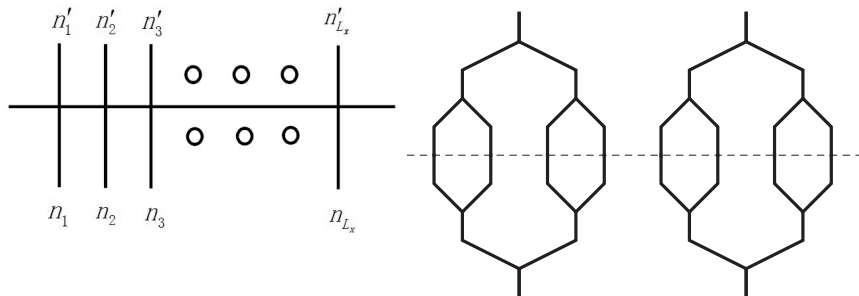


Figure: Graphical representation of the transfer matrix (left) and its successive coarse graining (right). See PRD 88 056005 and PRA 90, 063603 for explicit formulas.

Phase diagram

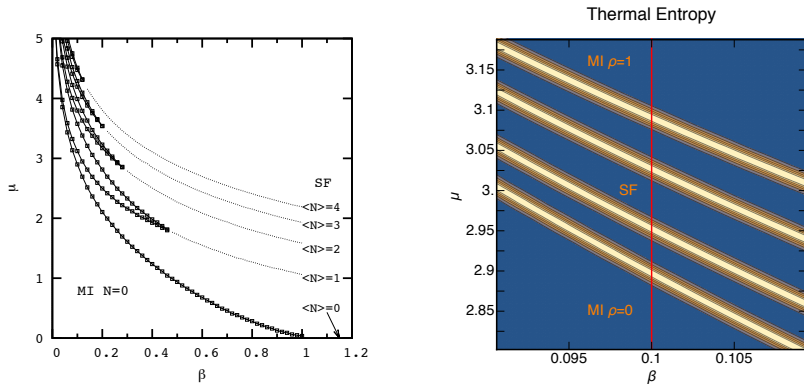


Figure: Mott Insulating “tongues” and Thermal entropy in a small region of the $\beta - \mu$ plane. Intensity plot for the thermal entropy of the classical XY model on a 4×128 lattice in the $\beta - \mu$ plane. The dark (blue) regions are close to zero and the light (yellow ochre) regions peak near $\ln 2$ (level crossing).

Entanglement entropy S_E (PRE 93, 012138 (2016))

We consider the subdivision of AB into A and B (two halves in our calculation) as a subdivision of the spatial indices.

$$\hat{\rho}_A \equiv \text{Tr}_B \hat{\rho}_{AB}; \quad S_{\text{EvonNeumann}} = - \sum_i \rho_{A_i} \ln(\rho_{A_i}).$$

We use blocking methods until A and B are each reduced to a single site.

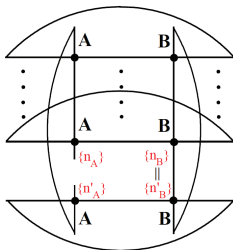


Figure: The horizontal lines represent the traces on the space indices. There are L_t of them, the missing ones being represented by dots. The two vertical lines represent the traces over the blocked time indices in A and B .

Rényi entanglement entropy

The n -th order Rényi entanglement entropy is defined as:

$$S_n(A) \equiv \frac{1}{1-n} \ln(\text{Tr}((\hat{\rho}_A)^n)) .$$

$\lim_{n \rightarrow 1^+} S_n =$ von Neumann entanglement entropy.

The approximately linear behavior in $\ln(N_S)$ is consistent with the Calabrese-Cardy scaling which predicts

$$S_n(N_S) = K + \frac{c(n+1)}{6n} \ln(N_S)$$

for periodic boundary conditions and half the slope ($\frac{c(n+1)}{12n}$) for open boundary conditions. The constant K is non-universal and different in the four situations considered ($n=1, 2$ with PBC and OBC).



Time continuum limit

When $\beta_t \gg \beta_x$ we obtain the time continuum limit (Fradkin, Susskind, Kogut, Polyakov, ..) and a quantum rotor Hamiltonian on a lattice with β_x acting as the coupling between the spatial sites.

$$\hat{H} = \frac{\tilde{U}}{2} \sum_x \hat{L}_x^2 - \tilde{\mu} \sum_x \hat{L}_x - \tilde{J} \sum_{\langle xy \rangle} \cos(\hat{\theta}_x - \hat{\theta}_y), \quad (3)$$

with $\tilde{U} = 1/(\beta_t a)$, $\tilde{\mu} = \mu_{ch.}/a$ and $\tilde{J} = \beta_x/a$, the sum extending over sites x and nearest neighbors $\langle xy \rangle$ in space and a the time lattice spacing. Finite spin approximations are used (typically spin-1).

For $\tilde{U} \gg \tilde{J}$ and $\tilde{\mu} \simeq \tilde{U}/2$, the model can be approximated by a Bose Hubbard model with a **single** species of bosons

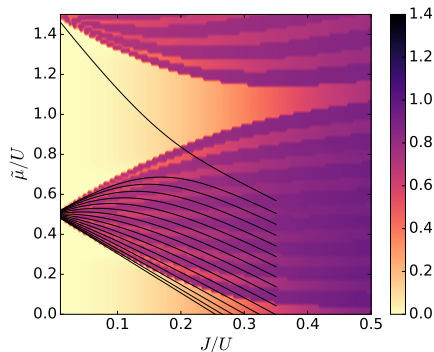
$$H_{BH} = \sum_x \left[\frac{\tilde{U}}{2} n_x^2 - \tilde{\mu} n_x - \tilde{J} (a_x a_{x+1}^\dagger + a_x^\dagger a_{x+1}) \right]$$



Central charge with cold atoms? PRA 96 023603 (2017), PRD 96 034514 (2017)

- Current experiments using cold bosonic atoms trapped in one-dimensional optical lattices can measure the second-order Rényi entanglement entropy S_2 (Greiner, Kaufman, Preiss, ...)
- Can we use it to verify detailed predictions of conformal field theory (CFT) and estimate the central charge c ?
- We propose an adiabatic preparation of the ground state at half-filling where we expect a CFT with $c = 1$. This can be accomplished with a very small hopping parameter J , in contrast to existing studies with density one where a much larger J is needed.
- We provide methods to estimate and subtract the classical entropy due to the experimental preparation and imaging
- We compare numerical calculations of S_2 for the classical $O(2)$ model with a chemical potential on a 1+1 dimensional lattice, and the quantum Bose-Hubbard model simulated in experiments.
- Can we check the Calabrese-Cardy scaling, $S_2 \simeq (c/8) \ln(N_S)$? 

Bose-Hubbard & $O(2)$ Phase Diagram



- $N_s = 16$ lattice
- Color is S_2 for time-continuum $O(2)$.
- The light lobes are Mott insulator regions
- The stripes are jumps in particle number
- In black are the particle number boundaries for BH

Experimental Proposal (PRA 96 023603 (2017))

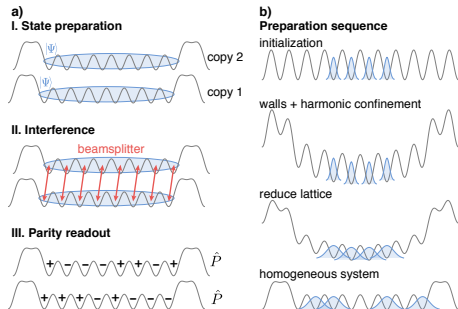
A way to set-up half-filling in the ground state

Left

- Two identical copies are made
- A beamsplitter operation is applied across the copies
- The resulting parities at each site in a copy give the quantum purity

Right

- A Mott state is prepared with N_p bosons.
- Harmonic confinement is imposed and boundary walls are created.
- J/U is tuned to the desired value.



Measurements of S_2

Using (Daley, Pichler, Schachenmayer and Zoller, PRL 109.020505):

$$\exp(-S_2) = \text{Tr}(\rho_{\mathcal{A}}^2) = \langle (-1)^{\sum_{x \in \mathcal{A}} n_x^{\text{copy}}} \rangle, \quad (4)$$

The probability for parity $(-1)^{n_x} = \pm 1$ is $(1 \pm \exp(-S_2))/2$. As S_2 increases, more cancellations occur and one needs on the order of $\exp(2S_2)$ measurements to overcome the fluctuations. Assuming N_s to be less than 16 (i. e., less than 8 particles at half-filling with an entropy per particle of order 0.05), the maximal measured S_2 is less than 1.1. For \mathcal{N} independent measurements, we find that the statistical error is

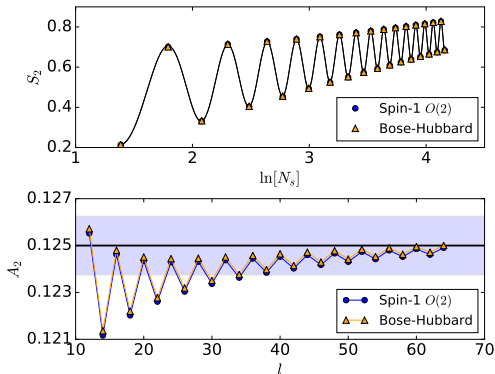
$$\sigma_{S_2} = \sqrt{(e^{2S_2} - 1)/\mathcal{N}}. \quad (5)$$

For the maximal value $S_2 = 1.1$, it takes about 800 measurements to reach $\sigma_{S_2} \simeq 0.1$. Due to the logarithmic growth of S_2 , the number of measurements only needs to increase like $N_s^{1/4}$ to maintain a desired accuracy, which is not a prohibitive growth.



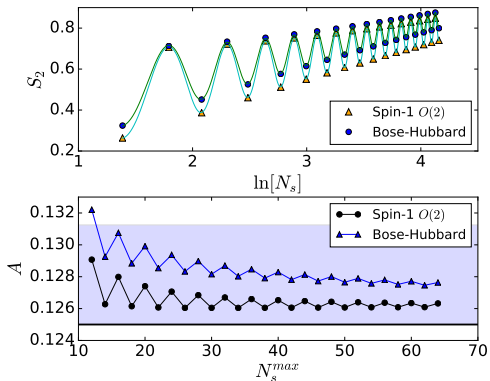
Results and Fits ($A_2 = c/8?$)

Rényi entropy and fit coefficient for BH and O(2) at $J/U = 0.005$



Results and Fits

Rényi entropy and fit coefficient for BH and O(2) at $J/U = 0.1$



Conclusion and Work to Do for the $O(2)$ model

- The $O(2)$ model can be quantum simulated with a single species BH model in the superfluid phase.
- It is possible with current experimental technology to observe the oscillations in S_2 .
- CFT provides functional forms for the Rényi entropy that make it possible to extract the central charge from experimental data.
- Look into efficient use of experimental data to improve the error.



The Abelian Higgs model on a 1+1 space-time lattice

a.k.a. lattice **scalar electrodynamics**. Field content:

- **Complex (charged) scalar field** $\phi_x = |\phi_x|e^{i\theta_x}$ on space-time sites x
- **Abelian gauge fields** $U_{x,\mu} = \exp iA_\mu(x)$ on the links from x to $x + \hat{\mu}$
- $F_{\mu\nu}$ appears when taking products of U 's around an elementary square (plaquette) in the $\mu\nu$ plane
- Notation for the plaquette: $U_{x,\mu\nu} = e^{i(A(x)_\mu + A(x+\hat{\mu})_\nu - A(x+\hat{\nu})_\mu - A(x)_\nu)}$
- $\beta_{pl.} = 1/e^2$ and κ is the **hopping** coefficient

$$\begin{aligned} \mathcal{S} = & -\beta_{pl.} \sum_x \sum_{\nu < \mu} \text{ReTr} [U_{x,\mu\nu}] + \lambda \sum_x \left(\phi_x^\dagger \phi_x - 1 \right)^2 + \sum_x \phi_x^\dagger \phi_x \\ & - \kappa \sum_x \sum_{\nu=1}^d \left[e^{\mu_{ch.} \delta(\nu,t)} \phi_x^\dagger U_{x,\nu} \phi_{x+\hat{\nu}} + e^{-\mu_{ch.} \delta(\nu,t)} \phi_{x+\hat{\nu}}^\dagger U_{x,\nu}^\dagger \phi_x \right]. \end{aligned}$$

$$Z = \int D\phi^\dagger D\phi DU e^{-\mathcal{S}}$$

Unlike other approaches (Reznik, Zohar, Cirac, Lewenstein, Kuno,...) we will not try to implement the gauge field on the optical lattice.



The large λ limit (finite λ will not be considered here)

$\lambda \rightarrow \infty$, $|\phi_x|$ is frozen to 1, or in other words, the Brout-Englert-Higgs mode becomes infinitely massive.

We are then left with compact variables of integration in the original formulation (θ_x and $A_{x,\hat{\nu}}$) and the Fourier expansions

$\exp[2\kappa_{\hat{\nu}} \cos(\theta_{x+\hat{\nu}} - \theta_x + A_{x,\hat{\nu}})] = \sum_{n=-\infty}^{\infty} I_n(2\kappa_{\hat{\nu}}) \exp(in(\theta_{x+\hat{\nu}} - \theta_x + A_{x,\hat{\nu}}))$

leads to expressions of the partition function in terms of discrete sums. We use the following definitions:

$$t_n(z) \equiv I_n(z)/I_0(z)$$

$$t_n(0) = \delta_{n,0}.$$

For z non zero and finite, we have $1 > t_0(z) > t_1(z) > t_2(z) > \dots > 0$
In addition for sufficiently large z ,

$$t_n(z) \simeq 1 - n^2/(2z)$$



Tensor Renormalization Group formulation

As in PRD.88.056005 and PRD.92.076003, we attach a $B^{(\square)}$ tensor to every plaquette

$$= \begin{cases} B_{m_1 m_2 m_3 m_4}^{(\square)} \\ t_{m_{\square}}(\beta_{pl}), & \text{if } m_1 = m_2 = m_3 = m_4 = m_{\square} \\ 0, & \text{otherwise.} \end{cases}$$

a $A^{(s)}$ tensor to the horizontal links

$$A_{m_{up} m_{down}}^{(s)} = t_{|m_{down} - m_{up}|}(2\kappa_s),$$

and a $A^{(\tau)}$ tensor to the vertical links

$$A_{m_{left} m_{right}}^{(\tau)} = t_{|m_{left} - m_{right}|}(2\kappa_{\tau}) e^{\mu}.$$

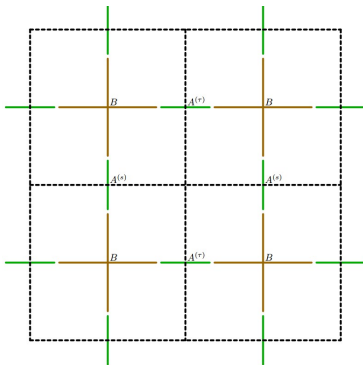
The quantum numbers on the links are completely determined by the quantum numbers on the plaquettes



$$Z = \text{Tr}[\prod T]$$

$$Z = \infty \text{Tr} \left[\prod_{h,v,\square} A_{m_{up}m_{down}}^{(s)} A_{m_{right}m_{left}}^{(\tau)} B_{m_1 m_2 m_3 m_4}^{(\square)} \right].$$

The traces are performed by contracting the indices as shown



The transfer matrix \mathbb{T}

$$\begin{aligned} \mathbb{B}_{(m_1, m_2, \dots, m_{N_S})}(m'_1, m'_2 \dots m'_{N_S}) &= t_{m_1}(2\kappa_\tau) \delta_{m_1, m'_1} t_{m_1}(\beta_{pl}) \times \\ &t_{|m_1 - m_2|}(2\kappa_\tau) \delta_{m_2, m'_2} t_{m_2}(\beta_{pl}) t_{|m_2 - m_3|}(2\kappa_\tau) \dots \\ &t_{m_{N_S}}(\beta_{pl}) t_{m_{N_S}}(2\kappa_\tau) \end{aligned}$$

Note that with this choice of open boundary conditions, the chemical potential has completely disappeared. If we had chosen different m 's at the end allowing a total charge Q inside the interval, we would have an additional factor $\exp(\mu Q)$. We next define a matrix \mathbb{A} as the product.

$$\begin{aligned} \mathbb{A}_{(m_1, m_2, \dots, m_{N_S})}(m'_1, m'_2 \dots m'_{N_S}) &= \\ &t_{|m_1 - m'_1|}(2\kappa_S) t_{|m_2 - m'_2|}(2\kappa_S) \dots t_{|m_{N_S} - m'_{N_S}|}(2\kappa_S) \end{aligned}$$

With these notations we can construct a symmetric transfer matrix \mathbb{T} . Since \mathbb{B} is diagonal, real and positive, we can define its square root in an obvious way and write the transfer matrix as

$$\mathbb{T} = \sqrt{\mathbb{B}} \mathbb{A} \sqrt{\mathbb{B}}$$



The time continuum limit and the energy spectrum

In the limit $\kappa_S = 0$, and if *both* κ_T and β_{pl} become large, at leading order in the inverse of these large parameters, the eigenvalues of \mathbb{T} are

$$\lambda_{(m_1, m_2, \dots, m_{N_s})} = 1 - \frac{1}{2} \left[\left(\frac{1}{\beta_{pl}} (m_1^2 + m_2^2 + \dots + m_{N_s}^2) + \frac{1}{2\kappa_T} (m_1^2 + (m_2 - m_1)^2 + \dots \dots + (m_{N_s} - m_{N_s-1})^2 + m_{N_s}^2) \right) \right]$$

In the case $1 \ll \beta_{pl} \ll \kappa_T$, we set the scale with the (large) gap energy $\tilde{U}_g \equiv 1/a\beta_{pl}$.

For $1 \ll \kappa_T \ll \beta_{pl}$, we tend to have strings of constant m but for large volume, the plaquette energy can take over (confinement).



The Hamiltonian for $1 \ll \beta_{pl} \ll \kappa_\tau$ and $m = 0, \pm 1$

We now use the spin-1 approximation ($m = 0, \pm 1$ or $n = 0, \pm 1$) to discuss the two cases.

For $1 \ll \beta_{pl} \ll \kappa_\tau$, We use the notation $\bar{L}_{(i)}^x$ to denote the first generator of the spin-1 rotation algebra at the site (i). The notation \bar{L} is used to emphasize that the spin is related to the m quantum numbers attached to the plaquettes, not to the charges n on the time links.

We define $\tilde{Y} \equiv (\beta_{pl}/(2\kappa_\tau))\tilde{U}_g$ and $\tilde{X} \equiv (\beta_{pl}\kappa_s\sqrt{2})\tilde{U}_g$ which are the (small) energy scales. The final form of the Hamiltonian \bar{H} for $1 \ll \beta_{pl} \ll \kappa_\tau$ is

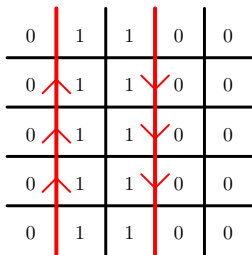
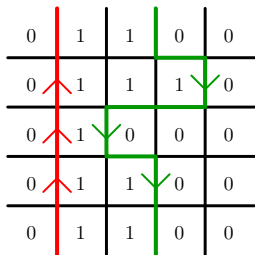
$$\bar{H} = \frac{\tilde{U}_g}{2} \sum_i (\bar{L}_{(i)}^z)^2 + \frac{\tilde{Y}}{2} \sum_i (\bar{L}_{(i)}^z - \bar{L}_{(i+1)}^z)^2 - \tilde{X} \sum_i \bar{L}_{(i)}^x .$$



Polyakov loop: definition

Polyakov loop, a Wilson line wrapping around the Euclidean time direction: $\langle P_i \rangle = \langle \prod_j U_{(i,j),\tau} \rangle = \exp(-F(\text{single charge})/kT)$; the order parameter for deconfinement.

With periodic boundary condition, the insertion of the Polyakov loop (red) forces the presence of a scalar current (green) in the opposite direction (left) or another Polyakov loop (right).



In the Hamiltonian formulation, we add $-\frac{\tilde{Y}}{2}(2(\bar{L}_{i^*}^Z - \bar{L}_{(i^*+1)}^Z) - 1)$ to H_{i^*}



Polyakov loop (Judah Unmuth-Yockey)

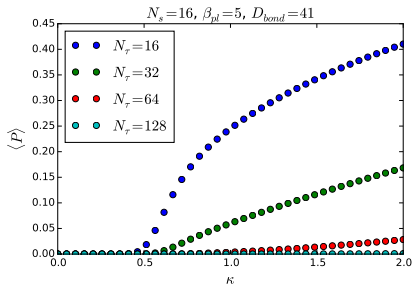
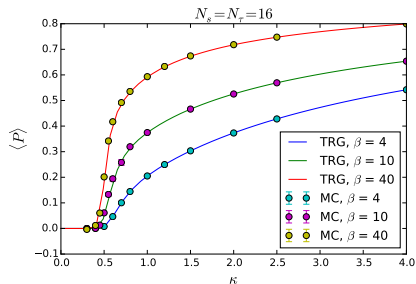


Figure: Left: comparison between TRG and MC. Right: TRG with fixed spatial length and various temporal lengths. Data like this was used to find the decay in the temporal length of the lattice. It was found to decay exponentially for large enough temporal lengths (see next slide).

Polyakov loop (Judah Unmuth-Yockey)

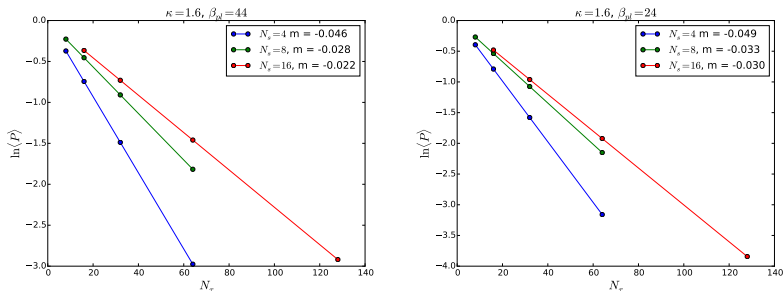


Figure: Here we see for different spatial sizes, the free energy for a static charge is different in each case for large N_T (very small T). The slope ΔE is a function of g^2 .



Conjectures

- For $g^2 N_s$ small enough $\Delta E \simeq a/N_s + bg^2 N_s$
- $\Delta E N_s = f(g^2 N_s^2)$ (data collapse)
- For large $g^2 N_s^2$, $f(g^2 N_s^2) \sim \sqrt{g^2 N_s^2}$
- ΔE stabilizes at large N_s at some value proportional to g

We use $g^2 = 1/\beta_{\text{plaquette}}$



Polyakov loop collapse (Judah Unmuth-Yockey)

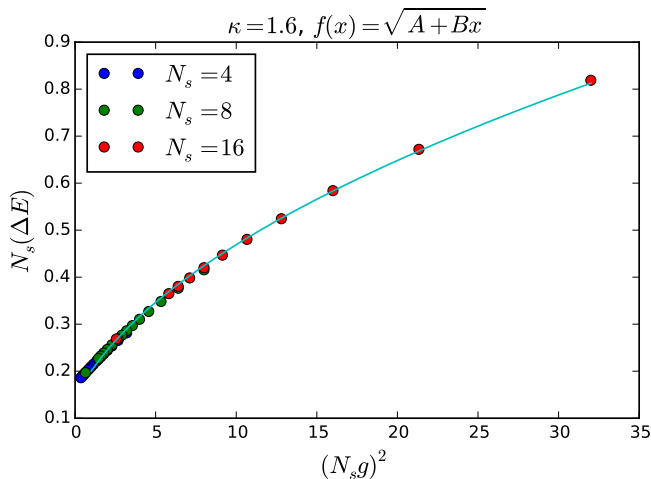


Figure: A fit to the universal curve of the form $\sqrt{A + Bx}$ (preliminary).



Two species Bose-Hubbard (PRD 92 076003)

The two-species Bose-Hubbard Hamiltonian ($\alpha = a, b$ indicates two different species, respectively) on square optical lattice reads

$$\begin{aligned}\mathcal{H} &= - \sum_{\langle ij \rangle} (t_a a_i^\dagger a_j + t_b b_i^\dagger b_j + h.c.) - \sum_{i,\alpha} (\mu + \Delta_\alpha) n_i^\alpha \\ &+ \sum_{i,\alpha} \frac{U_\alpha}{2} n_i^\alpha (n_i^\alpha - 1) + W \sum_i n_i^a n_i^b + \sum_{\langle ij \rangle \alpha} V_\alpha n_i^\alpha n_j^\alpha \\ &- (t_{ab}/2) \sum_i (a_i^\dagger b_i + b_i^\dagger a_i)\end{aligned}$$

with $n_i^a = a_i^\dagger a_i$ and $n_i^b = b_i^\dagger b_i$.

In the limit where $U_a = U_b = U$ and W and $\mu_{a+b} = (3/2)U$ much larger than any other energy scale, we have the condition $n_i^a + n_i^b = 2$ for the low energy sector. The three states $|2, 0\rangle$, $|1, 1\rangle$ and $|0, 2\rangle$ satisfy this condition and correspond to the three states of the spin-1 projection considered above.



Using degenerate perturbation theory

$$\begin{aligned}\mathcal{H}_{\text{eff}} &= \left(\frac{V_a}{2} - \frac{t_a^2}{U_0} + \frac{V_b}{2} - \frac{t_b^2}{U_0} \right) \sum_{\langle ij \rangle} L_i^z L_j^z \\ &+ \frac{-t_a t_b}{U_0} \sum_{\langle ij \rangle} (L_i^+ L_j^- + L_i^- L_j^+) + (U_0 - W) \sum_i (L_i^z)^2 \\ &+ \left[\left(\frac{pn}{2} V_a + \Delta_a - \frac{p(n+1)t_a^2}{U_0} \right) - \left(\frac{pn}{2} V_b \right. \right. \\ &\left. \left. + \Delta_b - \frac{p(n+1)t_b^2}{U_0} \right) \right] \sum_i L_i^z - t_{ab} \sum_i L_{(i)}^x\end{aligned}$$

where p is the number of neighbors and n is the occupation ($p = 2$, $n = 2$ in the case under consideration). \hat{L} is the angular momentum operator in representation $n/2$.



Matching the O(2) and BH spectra for large U

Matching: with the O(2) model, we need to tune the hopping amplitude as $t_\alpha = \sqrt{V_\alpha U/2}$ and have $\tilde{J} = 4\sqrt{V_a V_b}$, $\tilde{U} = 2(U - W)$, and $\tilde{\mu} = -(\Delta_a - V_a) + (\Delta_b - V_b)$.

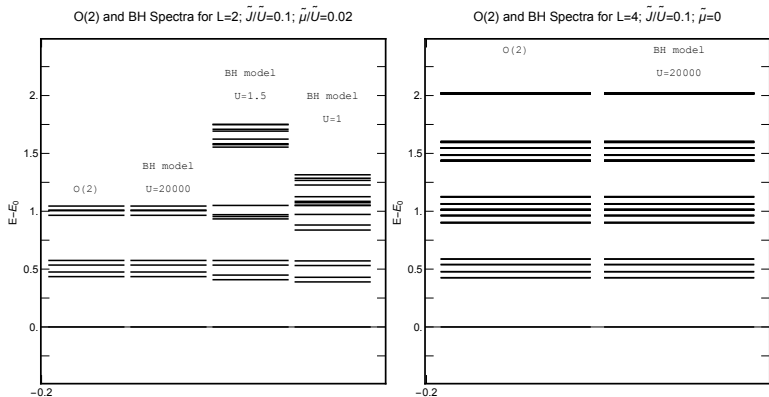
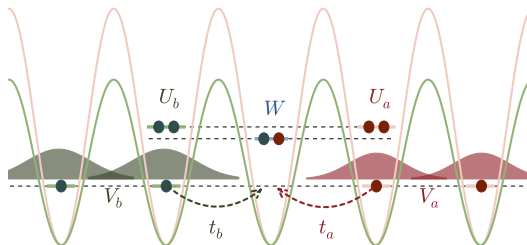


Figure: O(2) and Bose-Hubbard spectra for L=2 (left) and L=4 (right).



Optical lattice implementation (PRA 90 06303)

- The two-species: ^{87}Rb and ^{41}K Bose-Bose mixture where an interspecies Feshbach resonance is accessible (W).
- Species-dependent optical lattice are used in boson systems, which allows hopping amplitude of individual species to be tuned to desired values.
- The extended interaction, V_α , is present and small when we consider Wannier gaussian wave functions sitting on nearby lattice sites (Mazzarella et al. 2006)



Matching the Ab. Higgs model and BH spectra

$$\text{Matching: } t_a = t_b = 0, V_a = V_b = -\tilde{Y}/2, t_{ab} = \tilde{X}, \\ \tilde{U}_p = 2(U - W + 2V_{a(b)}), \Delta_{a(b)} = -2V_{a(b)}.$$

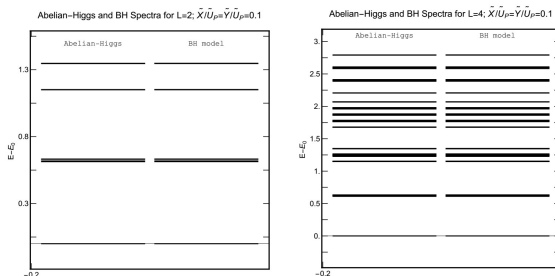


Figure: Abelian-Higgs model with $\tilde{X}/\tilde{U}_p = 0.1$, $\tilde{Y}/\tilde{U}_p = 0.1$ and the corresponding Bose-Hubbard spectra for $L = 2$ (top) and $L = 4$ (bottom).



Optical lattice implementation

- Ladder structure?

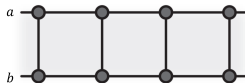


Figure: A ladder structure with a and b corresponding to the two sides of the ladder (right).

- Two species \rightarrow hyperfine states or physical ladder?

A physical ladder

- The two “species” of bosons previously invoked are the bosons in the two sides of the ladder.
- There is no tunneling along the two long sides of the ladder ($t_a = t_b = 0$) and there are exactly two bosons attached to each rung. This condition corresponds to the spin-1 approximation.
- The ladder can be setup in a way similar to the preparation of twin tubes in recent experiments. We start with a deep Mott ladder with one boson per site. We then make the potential more shallow along the rungs allowing t_{ab} to be non zero.
- The nearest neighbor interactions can be realized using Rydberg atoms (Zeihner et al. 1705.08372)



Checking the feasibility of the proposal with a simpler example (spin-1/2)

- With one boson per rung, we can realize a spin-1/2 system
- The range of the Rydberg interaction can be tuned in such a way that two neighbor atoms on the same side of the ladder feel an attractive interaction while if they are on opposite sides (but on neighbor rungs) the attraction is much weaker.
- We can use this simpler setup to quantum simulate the well studied quantum Ising model in a transverse field. This model has second order phase transition with known exponents.
- Spin-imaging is easy (up-down corresponds to the two sides of the ladder).



The “classical” Ising model

System of spins on a square lattice: $\sigma_{x,y} = \pm 1$

$$S = -\beta \sum_{(x,y)} \sigma_{x,y} (\sigma_{x+1,y} + \sigma_{x,y+1}) - h \sum_{(x,y)}$$

partition function: $Z = \sum_{\{\sigma\}} e^{-S}$

Second order phase transition (order-disorder) at self dual β_c :
 $\tanh(\beta_c) = \exp(-2\beta_c)$ which implies $\beta_c = \ln(1 + \sqrt{2})/2 = 0.4406\dots$

Transfer matrix exactly diagonalizable at finite volume (Kaufman)

Critical exponents are known exactly ($\nu = 1$, $\eta = 1/4$, $\gamma = 7/8$, ...)

Allows us to test renormalization group (RG) method

As quantum simulations are still made on relatively small lattices, it is convenient to study the finite size scaling dictated by the RG analysis of the second-order phase transition.



On a $L \times L$ lattice, the magnetic susceptibility is

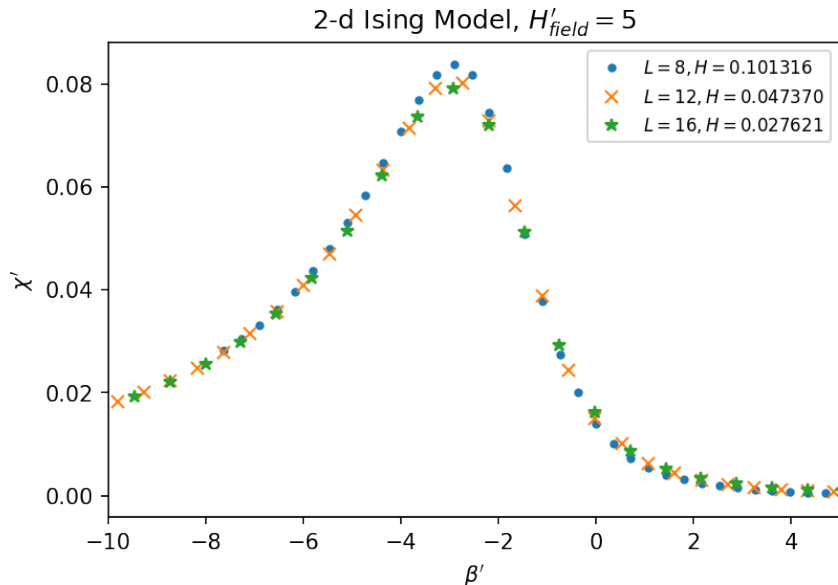
$$\chi^{class.} = \frac{1}{L^2} \sum_{\langle \mathbf{x}, \mathbf{y} \rangle} \langle (\sigma_{\mathbf{x}} - \langle \sigma_{\mathbf{x}} \rangle)(\sigma_{\mathbf{y}} - \langle \sigma_{\mathbf{y}} \rangle) \rangle \propto \xi^{2-\eta} \propto |\beta - \beta_c|^{-\gamma}$$

with ξ the correlation length and $\gamma = \nu(2 - \eta) = 1.75$

Under a RG transformation with a scale factor b , $L \rightarrow L/b$ and we obtain a data collapse by plotting $\chi^{class.'} = \chi^{class.} L^{-\gamma/\nu}$ versus $\beta' = L^{1/\nu}(\beta - \beta_c)/\beta_c$. A magnetic field is introduced to break the symmetry between the two vacua in the broken symmetry phase and is varied in order to keep $h' = hL^{15/8}$ constant. Numerical calculations by Jin Zhang.



Data collapse for the classical magnetic susceptibility



The “quantum” Ising model

It is possible to take the time continuum limit and keep the spatial lattice. This result into the quantum hamiltonian in one space dimension.

$$\hat{H} = -\lambda \sum_i \hat{\sigma}_i^z \hat{\sigma}_{i+1}^z - \sum_i \hat{\sigma}_i^x - h \sum_i \hat{\sigma}_i^z$$

where all the energies are expressed in units of the transverse magnetic field (the coefficient in front of $-\sum_i \hat{\sigma}_i^x$). In the ladder realization, this is proportional to the inverse tunneling time along the rungs. The zero temperature magnetic susceptibility is

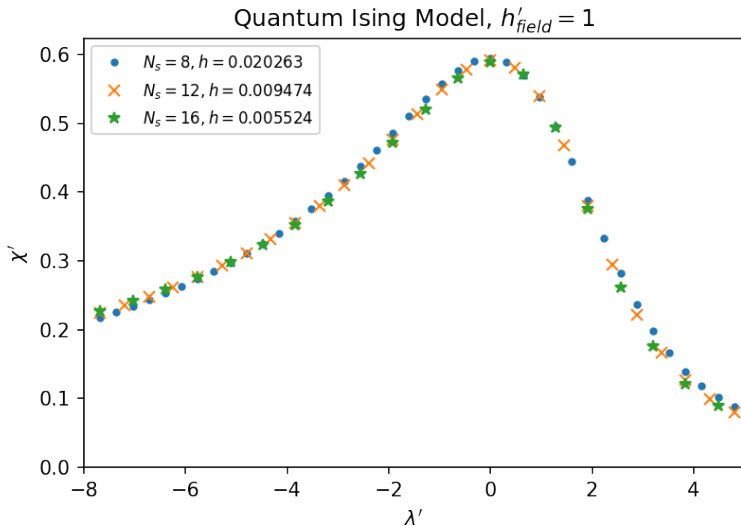
$$\chi^{quant.} = \frac{1}{L} \sum_{\langle i,j \rangle} \langle (\sigma_i - \langle \sigma_i \rangle)(\sigma_j - \langle \sigma_j \rangle) \rangle \propto \xi^{1-\eta} \propto |\lambda - 1|^{-\nu(1-\eta)}$$

where $\langle \dots \rangle$ are short notations for $\langle \Omega | \dots | \Omega \rangle$ with $|\Omega\rangle$ the lowest energy state of \hat{H} . Recent calculations by Jin Zhang show a nice data collapse.



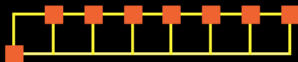
Data collapse for the quantum magnetic susceptibility:

$$\chi^{quant.'} = \chi^{quant.} L^{-(1-\eta)} \text{ versus } \lambda' = L^{1/\nu}(\lambda - 1)$$

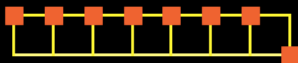


Looking at the vacuum wavefunction

$N_s=8; \lambda=1.50; H=0.20; \text{Prob.}=0.06$



$N_s=8; \lambda=1.50; H=0.20; \text{Prob.}=0.06$



$N_s=8; \lambda=1.50; H=0.20; \text{Prob.}=0.71$



Sudden expansion and thermalization (in progress)

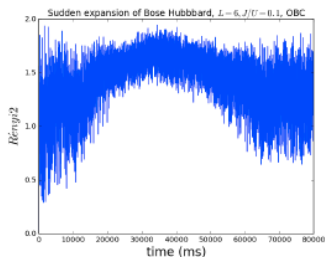


Figure: $S_2(t)$ for a sudden expansion (half-filling after the expansion), by Jin Zhang.

Conclusions

- We have proposed a **gauge-invariant** approach for the quantum simulation of the abelian Higgs model.
- The tensor renormalization group formulation allows reliable calculations of the **phase diagram and spectrum** in the limit $\lambda \rightarrow \infty$.
- Calculations of the **entanglement entropy** for the $O(2)$ model in the superfluid phase at increasing N_x are consistent with a **CFT of central charge 1**.
- Calculations of the **Polyakov loop** at finite N_x and small gauge coupling shows an interesting behavior (related to the KT transition of the limiting $O(2)$ model).
- We have proposed a Bose-Hubbard model that corresponds to the spin-1 version and proposed implementation on optical lattices.
- Proof of principle: data collapse for the quantum Ising model realized on a ladder.



Acknowledgements:

This research was supported in part by the Dept. of Energy under Award Numbers DOE grants DE-SC0010114, DE-SC0010113, and DE-SC0013496.

